Mesomorphism, Polymorphism, and Semicrystalline Morphology of Poly(Di-*n*-propylsiloxane)

Raluca I. Gearba,[‡,§] Denis V. Anokhin,[‡,§] Alexander I. Bondar,[‡] Yuli K. Godovsky,[†,⊥] Vladimir S. Papkov,[∥] Natalia N. Makarova,[∥] Sergei N. Magonov,[#] Wim Bras,[○] Michel H. J. Koch,[⊗] Francis Masin,[¶] Bart Goderis,[◆] and Dimitri A. Ivanov*[,‡,§]

Laboratoire de Physique des Polymères, CP-223, Université Libre de Bruxelles, Bld. du Triomphe, B-1050, Brussels, Belgium, Karpov Institute of Physical Chemistry, 10 Vorontsovo Pole, 103064 Moscow, Russia, Nesmeyanov Institute of Organoelement Compounds, Russian Academy of Sciences, 28 Vavilov Str., 117813 Moscow, Russia, Veeco Metrology Group, 112 Robin Hill Road, Santa Barbara, California 93117, Netherlands Organization for Scientific Research (NWO), DUBBLE-CRG/ESRF, B.P. 220, F-38043 Grenoble Cedex, France, European Molecular Biology Laboratory, EMBL c/o DESY, Notkestrasse 85, 22603 Hamburg, Germany, Matière Condensée et Résonance Magnétique, CP-223, Université Libre de Bruxelles, Bld. du Triomphe, B-1050, Brussels, Belgium, and Chemistry Department, Catholic University of Leuven, Celestijnenlaan 200F, 3001 Heverlee-Leuven, Belgium

Received June 22, 2005; Revised Manuscript Received November 10, 2005

ABSTRACT: The crystalline structure and semicrystalline morphology of poly(di-*n*-propyl siloxane), PDPS, were studied with powder and fiber X-ray diffraction, differential scanning calorimetry, solid-state nuclear magnetic resonance and atomic force microscopy (AFM). PDPS exhibits two crystalline phases, α (−45.5 °C < *T* < 62 °C) and *β* (*T* < −45.5 °C), and a hexagonal columnar mesophase which is stable in a broad temperature range between 62 and 197 °C. The low-temperature crystalline phase *β* is found to be monoclinic with lattice parameters $a = 20.60$ Å, $b = 19.22$ Å, $c = 4.95$ Å, $\gamma = 93.1°$. The α crystalline phase has a pseudo-tetragonal unit cell with $a = b = 19.15$ Å and $c = 5.00$ Å and is characterized by monoclinic *C*2/*c* (No. 15) group symmetry. In the refined unit cell ($R_{wp} = 0.127$) the PDPS chains adopt a planar cis−trans conformation with the plane of the chain parallel to the *b* axis. The semicrystalline morphology of the α crystal was studied with AFM. The crystallization of PDPS from the hexagonal mesophase results in very thick (100−150 nm thick) crystalline lamellae, which implies that the chains are fully extended in the crystal. This feature, which is found in few polymers, makes PDPS similar to such systems as HDPE at high pressure or 1,4-*trans*-poly(butadiene).

I. Introduction

Inorganic polymers have attracted a continuously growing interest during the past decades due to their various technological applications. In particular, siloxanes are widely employed as lubricants, resins, greases, and elastomers. Apart from their practical importance these polymers display interesting thermal behavior. For instance, poly(di-*n*-alkysiloxanes), with two to six carbon atoms per side chain, form hexagonal columnar mesophases although there are no mesogenic moieties in the chemical structure. Linear poly(di-*n*-propylsiloxane), PDPS, is the second member in this family of flexible mesomorphic nonmesogenic poly(di-*n*-alkylsiloxanes).[1,2] The thermal stability interval of the mesomorphic state in PDPS is about 100 °C broader than that in poly(di-*n*-ethylsiloxane), PDES, which confirms the very strong dependence of the isotropization temperature on the side-chain length already documented for the first members of the family.[3,4] PDPS exhibits two crystalline modifications[3−10] and a mesophase for which a hexagonal columnar packing of the chains was suggested.[2,9] The high-temperature crystalline modification of PDPS was first described by Petersen et al.[11] as tetragonal with $a = b = 9.52$Å and $c = 9.4$Å, while the low-temperature modification was assumed to be monoclinic, but no lattice parameters were reported.[3−9] It was also suggested that the low-temperature modification could be a mixture of a tetragonal and a monoclinic phase.[8]

Early studies[11] established that in the semicrystalline structure PDPS forms chain-folded lamellar crystals with thicknesses around 20 nm. However, more recent small-angle neutron scattering work has shown existence of partly disentangled chains in the columnar mesophase,[12] which suggests a tendency to form extended or nearly-extended chain crystals.

Upon cooling from the isotropic melt, crystallization in bulk PDPS is rather fast making it difficult to obtain amorphous samples even by rapid quenching. Similarly, the rate of mesophase formation upon cooling of PDPS is so high that bulk crystallization always proceeds from the mesomorphic state. The critical molecular mass for mesophase formation in PDPS is about 10 kg/mol[3,4] or, about three times lower than that for PDES (28 kg/mol).[13,14] This difference is likely to result from an increase in chain stiffness as a function of the length of the side groups.[1] As for PDES, a linear relationship between the isotropization temperature and reciprocal molecular mass was established,[1−3] which is closely related to the low isotropization enthalpy and the rather high interfacial energy of the mesophase

* To whom correspondence should be addressed. E-mail: dimitri.ivanov@uha.fr.
† Unexpectedly passed away on May 23, 2005.
‡ Laboratoire de Physique des Polymères, CP-223, Université Libre de Bruxelles.
§ Present address: Institut de Chimie des Surfaces et Interfaces (ICSI), UPR CNRS 9069, 15 rue Jean Starcky, B.P. 2488, 68057 Mulhouse Cedex, France.
⊥ Karpov Institute of Physical Chemistry.
∥ Nesmeyanov Institute of Organoelement Compounds, Russian Academy of Sciences.
Veeco Metrology Group.
○ Netherlands Organization for Scientific Research (NWO).
⊗ European Molecular Biology Laboratory.
¶ Matière Condensée et Résonance Magnétique, CP-223, Université Libre de Bruxelles.
◆ Catholic University of Leuven.

10.1021/ma0513315 CCC: $33.50
Published on Web 01/11/2006

Table 1. Structural Characteristics and Thermal Behavior of PDPS Samples[a]

N	$M_w \times 10^{-3}$ [g]	*L* [nm]	T_g [°C]	T_{cr-cr} [°C]	ΔH_{cr-cr} [J/g]	T_m [°C]	ΔH_m [J/g]	T_i [°C]	ΔH_i [J/g]
I	87	163	−109.0	−45.5	31	62.0	24	197	≈1.2
II	27	50	−109.0	−76.0	1.2	46.0	13	69	<0.5

[a] Key: *N*, sample number; M_w, molecular mass; *L*, length of the chain in the cis-trans conformation; T_g, glass transition temperature; T_{cr-cr}, low-temperature polymorphic transition; T_m, melting temperature; T_i, clearing point; ΔH, enthalpy variation.

lamellae.[1−3] On the basis of this linear relationship, and on a more general analogy between the mesophase behavior of PDES and PDPS, it was proposed that the chains have an extended conformation in the mesophase lamellae.[1,2] Subsequent crystallization of these extended chain mesomorphic lamellae can be followed by the formation of extended chain crystalline lamellae. Thus, so far, both folded-chain and extended-chain morphology have been proposed for PDPS crystallization. It should be noted that spherulitic morphologies have not been observed in these polymers. This could indicate that crystal growth proceeds anisotropically and possibly uses the mesomorphic ordering as a template. A similar situation was recently reported for a low molecular mass star-shaped mesogen.[15]

Although some data on the PDPS crystalline phases are available, detailed structural information is still missing. Moreover the data on the semicrystalline and mesophase morphologies of PDPS are also very scarce in the literature. So far, only a preliminary atomic force microscopy (AFM) characterization of the crystalline and mesophase morphology of PDPS, and its evolution in the course of melting and crystallization, has been reported.[16] To fill this knowledge gap, we have undertaken a study on the structure of the PDPS crystalline modifications and columnar mesophase at different temperatures by means of X-ray fiber diffraction. The temperature-dependent evolution of the lattice parameters was followed in time-resolved experiments using X-ray powder diffraction on a synchrotron radiation beamline. Further insights in the semicrystalline morphology of PDPS are obtained with solid-state nuclear magnetic resonance (NMR) and AFM. Our microscopy studies were focused on the change in sample morphology upon the crystal-mesophase transition between 20 and 130 °C.

II. Materials and Methods

II.1. Materials. Two PDPS samples with different molecular mass were prepared by anionic ring-opening polymerization of hexapropylcyclotrisiloxane. This procedure is described elsewhere.[3,4,8,9] The samples were subsequently fractionated by precipitation at 25 °C using a toluene−methanol mixture. The molecular weights (M_w), determined by light scattering in toluene at 25 °C, were 87 000 (I) and 27 000 (II). The corresponding degrees of polymerization are 670 and 207, respectively. The characteristic transition temperatures of the samples are listed in Table 1. All results given below correspond to sample I unless specified otherwise.

II.2. Methods. II.2.1. Differential Scanning Calorimetry (DSC). Phase transitions in PDPS samples were studied with a Mettler Toledo 822[e] heat flux DSC equipped with a LN_2 cooling system. The instrument was previously calibrated using the melting temperatures and enthalpies of In and Zn.

II.2.2. Density measurements were performed at ambient temperature using a density gradient column filled with a mixture of 2-propanol/water.

II.2.3. X-ray diffraction on oriented samples was performed on beamline BM26B at the European Synchrotron Radiation Facility in Grenoble, France, using 10 keV X-rays.[17] The data were collected in transmission geometry using relatively large X-ray sensitive Fuji image plates which were scanned with a pixel size of 98 × 98 μm^2. The temperature was controlled by a Linkam heating stage operated under a LN_2 flow.[18] The modulus of the scattering vector $\boldsymbol{s}$ ($s = 2(\sin\theta)/\lambda$, where θ is the Bragg angle and λ is the wavelength) was calibrated using three diffraction orders of silver behenate.[19] Fibers with a diameter of 0.7 mm were obtained by extruding the material in the liquid crystalline state with a home-build miniextruder. The material can easily be oriented in the mesophase and the orientation is preserved during subsequent crystallization on cooling.

Time- and temperature-resolved X-ray diffraction experiments on powder samples were conducted at the European Molecular Biology Laboratory, DESY, Hamburg, Germany. SAXS and WAXS patterns were collected in transmission geometry, using two delay readout detectors connected in series. The temperature of the samples was controlled by a Mettler FP82 heating stage coupled to a FP90 processor. The experiments were performed during heating and cooling cycles at 10 °C·min^{-1} in successive frames of 12 s each. The *s*-axis was calibrated according to the conventional method[20] using silver behenate for small angles and benzoic acid for wide angles.

Powder X-ray diffraction measurements at ambient temperature were performed in $\theta-\theta$ geometry in reflection with a Bruker D8 Advance diffractometer equipped with a Göbel mirror. The X-ray tube with a copper anode was operated at 40 kV and 40 mA. The experiments were carried out in a vacuum using a motorized MRI X-ray reflectivity chamber. The diffraction intensity was recorded with a scintillation counter.

II.2.4. X-ray Data Analysis and Structure Modeling. The *Discover* and *Reflex* modules of "Materials Studio" package (Accelrys Inc.) were used to build and refine the crystal structure of PDPS. The refinement was performed by minimizing the weighted profile *R* factor, R_{wp}, defined as follows:

$$R_{wp} = \sqrt{\frac{\sum w_i(cI_{sim}(2\theta_i) - I_{exp}(2\theta_i) + I_{back}(2\theta_i))^2}{\sum w_i(I_{exp}(2\theta_i))^2}} \qquad (1)$$

In eq 1 $w_i = 1/I_{exp}(2\theta_i)$ is a weighting function, *c* is a scaling factor, $I_{sim}(2\theta_i)$ is the simulated intensity, $I_{exp}(2\theta_i)$ and $I_{back}(2\theta_i)$ are the measured intensities corresponding to the crystalline and amorphous regions of the sample. For refinement, the simulated annealing method implemented in the *Powder Solve* module was used. The simulated diffraction curve was polarization-Lorentz corrected. The polarization effects were accounted for by multiplying the intensity by $p + (1 - p)\cos^2 2\theta$, where *p* is the polarization factor. The Lorentz factor, which accounts for the different proportions of the full diffraction cone that are intercepted at different scattering angles by a constant vertical aperture, was taken as $1/(\sin\theta \sin 2\theta)$.

The sample crystallinity was computed from the fit to the powder X-ray diffractogram as a ratio of the crystalline intensity over the total diffracted intensity, where all disorder parameters, including the overall isotropic temperature factor *B*, were set to zero.

II.2.5. Atomic Force Microscopy. AFM experiments were carried out with a Nanoscope IIIa MultiMode AFM (Veeco Metrology Group, Santa Barbara, CA) in tapping mode, which is most suitable for soft materials imaging. In previous AFM studies on PDES and other mesomorphic polymers it was demonstrated that images in tapping mode can reveal morphological detail of both crystalline and liquid crystalline regions.[10,16] The utility of phase imaging has been also demonstrated for high-temperature AFM studies of polymers such as polyethylene,[21,22] poly(ϵ-caprolactone),[23] poly(ethylene terephthalate),[24] polytrimethylene terephthalate[25] and mesomorphic polysiloxane.[10,26] In the present work, a commercial heating stage[26,27] coupled to a vertical-engage J-scanner was employed. Tapping mode Si probes (220 μm in length, resonant frequency 150−200 kHz, stiffness ca. 40 N/m)

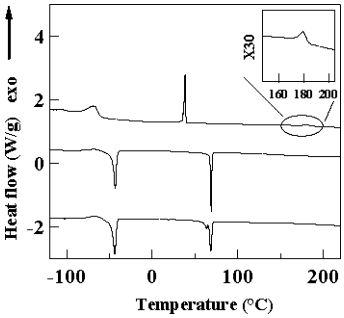

Figure 1. DSC curves recorded during successive heating and cooling cycles at 10 °C·min^{-1}. From bottom to top: first heating, second heating, and cooling. The inset shows a magnified part of the cooling curve, where the exothermic isotropic to mesophase transition occurs.

were used. The amplitude of the free-oscillating cantilever, A_0, was chosen between 50 and 100 nm. Imaging was performed in both light and hard tapping modes, whereby the set-point amplitude, A_{sp}, were $(0.8-0.9)A_0$ and $(0.4-0.5)A_0$, respectively. Light tapping was used for high-resolution imaging of the top surface structures, whereas discriminative visualization of amorphous, mesophase, and crystalline regions was performed in hard tapping. Thin layers of PDPS were prepared by rubbing the material on a plasma-cleaned silicon surface.

II.2.6. Solid-State NMR. NMR experiments were performed using a MSL300 WB Bruker spectrometer operating at 59.6 MHz for silicon. The ^{29}Si NMR spectra were collected using magic angle spinning (MAS) conditions with high-power proton dipolar decoupling (DD). The measurements were carried out using a Brüker MAS probe, the diameter of the rotor being 4 mm. The spinning frequency was 1372 Hz with 5 μs time for the pulse at 90°. The recycling time, D_0, for the DD-MAS experiments, was 100 s. The cross-polarization wide-line separation (CP−WISE) ^{1}H/^{29}Si spectra were collected using a 400 WB Bruker Advance spectrometer. The free induction decay (FID) measurements were performed using a sequence of echo pulses at 90° with a duration of 2 μs delayed by 25 μs. The chemical shifts were calibrated with respect to tetramethysilane (TMS). For the high-temperature crystalline phase the spectra were recorded at 292 K.

III. Results

III.1. DSC Measurements. DSC traces obtained during cooling and heating ramps between −120 and 220 °C are shown in Figure 1. The characteristic phase transition parameters are summarized in Table 1. We observe that there are three reversible endothermic transitions on heating. Since the enthalpy change associated with the high-temperature transition (197 °C) is at least 1 order of magnitude smaller than those of the other transitions, we tentatively assigned this to the clearing point. The low-temperature endotherm (−45.5 °C) was assigned to a polymorphic crystal−crystal transition and the one at 62 °C to melting of the high-temperature crystal modification. We define the high- and low-temperature crystal modifications as α and β, respectively, and the mesophase as Col_h. PDPS exhibits an exceptionally broad temperature stability window of the mesophase (more than 135 °C). A comparison between thermograms obtained on cooling and on heating reveals large hysteresis effects, which are typical of first order phase transitions in polymers. The hysteresis effect stretches over approximately 15 °C for the isotropic to mesophase transition and approximately 25 °C for both the mesophase to α and the α to β transitions.

III.2. X-ray Diffraction. A variety of X-ray diffraction and scattering techniques has been applied to the samples in order to determine the crystalline and mesomorphic structure and to characterize the thermal behavior of the phases. In this section

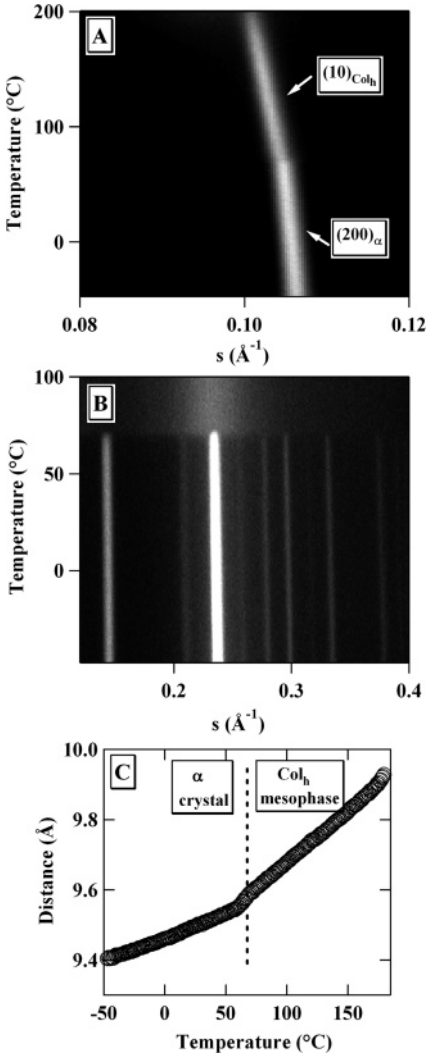

Figure 2. Time- and temperature-resolved synchrotron X-ray diffraction patterns acquired during heating at 10 °C·min^{-1} from −50 to +190 °C (the mesophase temperature range is between ca. 62 and 197 °C). Key: (A) SAXS range; (B) WAXS range. The temperature evolution of the repeat distance d_{hkl} shows a change in the slope at the crystal to mesophase transition (C).

we discuss the results of temperature-resolved X-ray diffraction experiments on isotropic samples (powders) and fiber diffraction experiments on oriented samples.

III.2.1. Temperature-Resolved Powder Diffraction. Figure 2A displays the small-angle X-ray scattering intensity during heating from −50 to +200 °C at 10 °C·min^{-1}. The intensity is represented in gray scale and is displayed as a function of the norm of the scattering vector and temperature. The corresponding wide-angle intensity given in Figure 2B shows that all sharp reflections disappear above approximately 62 °C indicating that the sample passes from the α crystalline modification in the mesophase. In Figure 2C, we show the temperature evolution of the *d* spacing of the 200 reflection of the α crystal, $d_{200}(\alpha)$, and the 10 reflection of the mesophase, $d_{10}(Col_h)$. A change in the slope can be observed upon the α crystal to the mesophase transition (Figure 2C). The calculated linear thermal expansion coefficients of the lateral unit cell parameter are 1.4×10^{-4} and 3.1×10^{-4} K^{-1} for the α and Col_h phases, respectively. The lateral expansion of the mesophase is more than twice as fast as that of the crystal.

III.2.2. X-ray Fiber Diffraction. III.2.2.1. A fiber diffraction pattern of the mesophase at 100 °C is shown in Figure 3. There

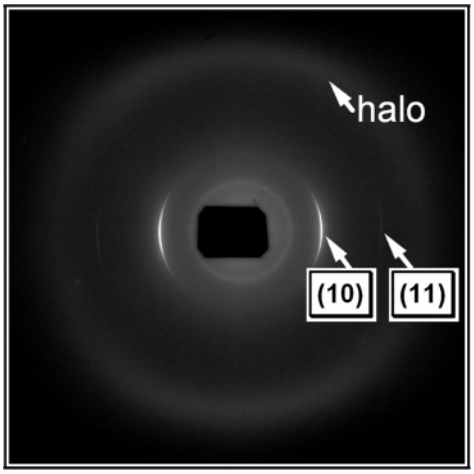

Figure 3. X-ray fiber diffraction pattern of the PDPS mesophase, recorded at 100 °C. The fiber axis is vertical.

are two equatorial reflections in the small-angle region with spacings given by the ratio 1:$\sqrt{3}$. These can be indexed to the (10) and (11) reflections of a columnar hexagonal mesophase, Col_h. The lattice parameter was found to be 11.2 Å. The first small-angle peak is due to the Kapton film used to fix the sample in the beam. The wide-angle region of the same sample displays only one broad peak (halo) located at $s = 0.22$ Å^{-1}. The presence of this halo is typically attributed to disordered alkyl side chains. In contrast with the results reported for the mesophase of PDES[28,29] there are no reflections revealing order along the chain axis.

III.2.2.2. A typical diffraction pattern of the α crystalline modification recorded at ambient temperature is presented in Figure 4A. The pattern shows a large number of sharp reflections but a rather low intensity amorphous halo. This is unusual for polymers and indicates a high degree of crystallinity, which is not uncommon in low molecular weight compounds. In total, 34 independent reflections distributed over three layer lines (denoted in the figure as $l = 0, \pm 1, \pm 2$) were analyzed. The indexing for the equatorial section of the pattern (Figure 4C) can be made to a tetragonal lattice. Similarly to the β_2 polymorph of PDES,[30] the meridional peak is absent in the first layer line and observed only in the second one. This is illustrated in Figure 4D, where the azimuthal intensity of the first (i.e., small angle) peaks in the fist and second layer lines is plotted. The proposed indexation of the reflections is given in Table 2. The lattice parameters evaluated from a fit of all *d* spacings are as follows: $a = b = 19.15$ Å and $c = 5.00$ Å. It is noteworthy that, according to this indexation scheme, the *a* and *b* parameters are doubled and the *c* parameter is approximately halved compared to the values reported previously by Petersen et al.[11]

The size of the crystallites was estimated employing conventional line broadening analysis. However, it was found that both the widths of the most intense equatorial and meridional peaks are limited by the instrumental resolution as determined from the peak profiles of a standard sample (Si powder). This

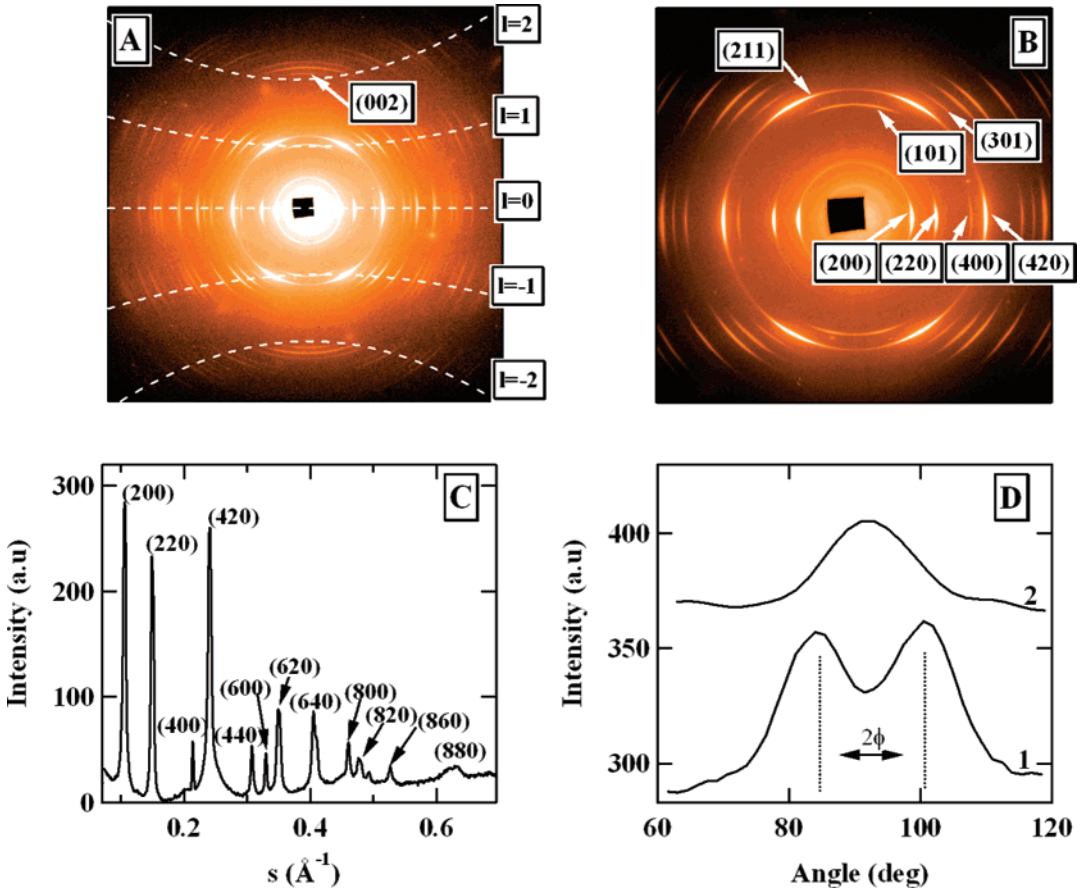

Figure 4. (A) X-ray fiber diffraction pattern corresponding to the α polymorph of PDPS. The reflections are arranged on layer lines with $l = 0$, ± 1, ± 2. The positions of the layer lines are indicated by dashed lines. (B) magnification of the same pattern in the low angle range. (C) Equatorial diffraction intensities of the pattern in part A. (D) Azimuthal distribution of the diffracted intensity corresponding to 101 (1) and 002 reflections (2). For clarity, the curves are vertically offset.

Table 2. X-ray Fiber Diffraction Data Corresponding to the α Polymorph of PDPS Measured at Room Temperature

h k l[a]	d_{exp} [Å]	d_{calc} [Å]	I_{obs}[b]
2 0 0	9.52	9.58	VS
2 2 0	6.76	6.77	VS
4 0 0	4.79	4.79	M
4 2 0	4.28	4.28	VS
4 4 0	3.41	3.39	M
6 0 0	3.20	3.19	M
6 2 0	3.03	3.03	S
6 4 0	2.68	2.66	S
8 0 0	2.41	2.39	M
8 2 0	2.35	2.32	M
6 6 0	2.29	2.26	W
8 4 0	2.17	2.14	W
8 6 0	1.94	1.92	W
1 0 1	4.83	4.83	S
2 1 1	4.31	4.32	VS
3 0 1	3.95	3.93	M
3 2 1	3.64	3.64	S
4 1 1	3.40	3.40	S
4 3 1		3.04	
5 0 1	3.04	3.04	S
6 1 1	2.66	2.66	M
5 4 1	2.56	2.57	M
6 3 1	2.50	2.48	W
6 5 1	2.22	2.20	W
8 1 1	2.15	2.15	W
7 4 1		2.15	
8 3 1	2.07	2.05	W
0 0 2	2.49	2.50	M
2 0 2	2.41	2.42	M
2 2 2	2.34	2.34	W
3 1 2		2.31	
4 0 2	2.21	2.21	W
4 2 2	2.16	2.16	W
3 3 2		2.18	
4 4 2	2.01	2.01	W
6 0 2	1.97	1.97	W
5 3 2		1.99	
6 2 2	1.93	1.93	W
6 4 2	1.82	1.82	W
7 1 2		1.84	

[a] Since the *d* spacings of *hkl* and khl reflections are identical for the pseudo-tetragonal unit cell, only *hkl* reflections are indicated in the table for the sake of brevity. [b] Intensity of reflections: VS-very strong, S-strong, M-medium, W-weak.

resolution limitation implies that the crystallite size in the directions perpendicular and parallel to the chain axis exceeds 31 nm.

The mass density, ρ, of the α crystal was evaluated as

$$\rho = \frac{M_{ru}Z}{N_A V_{unit\ cell}} \quad (2)$$

where in this case $V_{unit\ cell} = abc = a^2c$, M_{ru} is the molecular mass of the repeating unit, and Z is the number of chains per unit cell. Assuming that the unit cell accommodates four chains, a density of 0.94 ± 0.02 g/cm^3 was found, which is close to the experimental density values of 0.960 g/cm^3 and the previously reported value of 0.95 ± 0.02 g/cm^3.[11] Such close agreement between the densities of the crystal and the bulk sample indicates a high crystallinity of the material at ambient temperature.

III.2.2.3. An X-ray diffraction pattern corresponding to the β crystal recorded at −80 °C is shown in Figure 5. The number of observed diffraction peaks is higher than in the pattern of the α phase, thus suggesting a lower symmetry of the β phase. The equatorial peaks (Figure 5C) can be indexed to a monoclinic unit cell with a = 20.60 Å, b = 19.22 Å, c = 4.95 Å, γ = 93.1°. A small difference between a and b together with γ slightly deviating from 90° produces splitting of the peaks visible in the sections of the pattern along the equator and along the first layer line (Figure 5C,D). The experimentally determined diffraction peaks and their possible indexations are summarized in Table 3. The mass density estimated from eq 2 using $V_{unit\ cell} = abc \sin\gamma$ = 0.88 ± 0.02 g/cm^3, i.e., somewhat lower than that of the α phase.

Table 3. X-ray Fiber Diffraction Data Corresponding to the β Polymorph of PDPS Measured at −80 °C

h k l	d_{exp} [Å]	d_{calc} [Å]	I_{obs}
2 0 0	10.27	10.29	VS
0 2 0	9.65	9.59	VS
2 −1 0	9.24	9.27	VS
1 2 0	8.47	8.52	VS
2 2 0	6.88	6.84	VS
3 −1 0	6.63	6.57	VS
1 −3 0	6.19	6.20	VS
4 0 0	5.13	5.14	VS
2 4 0	4.20	4.26	VS
5 −1 0	4.08	4.07	M
−3 4 0		4.03	
5 −2 0		3.86	
−1 5 0	3.77	3.81	M/W
5 2 0		3.71	
−3 5 0	3.43	3.43	W
4 4 0		3.42	
3 5 0	3.31	3.27	M
5 4 0	3.05	3.04	S
4 −6 0	2.80	2.78	S
3 6 0		2.84	
6 5 0	2.53	2.49	M
1 −1 1	4.69	4.68	S
1 1 1	4.65	4.65	S
1 2 1	4.25	4.28	VS
2 2 1	4.00	4.01	S
3 0 1		4.01	
2 −2 1		4.08	
3 2 1	3.70	3.66	M
3 −2 1		3.74	
4 0 1	3.56	3.57	S
4 1 1		3.48	
3 −3 1		3.45	
1 −4 1	3.41	3.42	M
3 −4 1	3.12	3.13	M
5 1 1		3.10	
5 −1 1		3.14	
5 −3 1	3.86	3.88	M
3 1 1		3.90	
5 −4 1	2.73	2.69	S
5 4 1	2.61	2.59	W
0 0 2	2.45	2.47	W
0 1 2	2.42	2.45	W
−1 0 2		2.46	
1 −2 2	2.37	2.38	W
1 2 2		2.38	
2 2 2	2.32	2.33	W
2 −2 2		2.34	
3 −2 2	2.28	2.27	W
−2 3 2		2.26	
3 2 2		2.25	

III.3. NMR Measurements. Figure 6A shows a typical ^{29}Si DD-MAS spectrum of PDPS, in which two major peaks, with chemical shifts of −25.1 and −23.5 ppm, can be seen. Also two minor peaks at −0.536 and −46.51 ppm are present. These can be related to the rotation bands of the first main peak (note that the second main peak does not show any rotation bands). The presence of two major resonant peaks can indicate either the existence of different kinds of magnetic environment for Si atoms or originate from two regions of different mobility. In the latter case, the difference in chemical shifts of the main peaks may be due to the fact that the average magnetic field at the positions of Si atoms in the two phases is not identical. Therefore, the first resonant peak −25.1 ppm would correspond

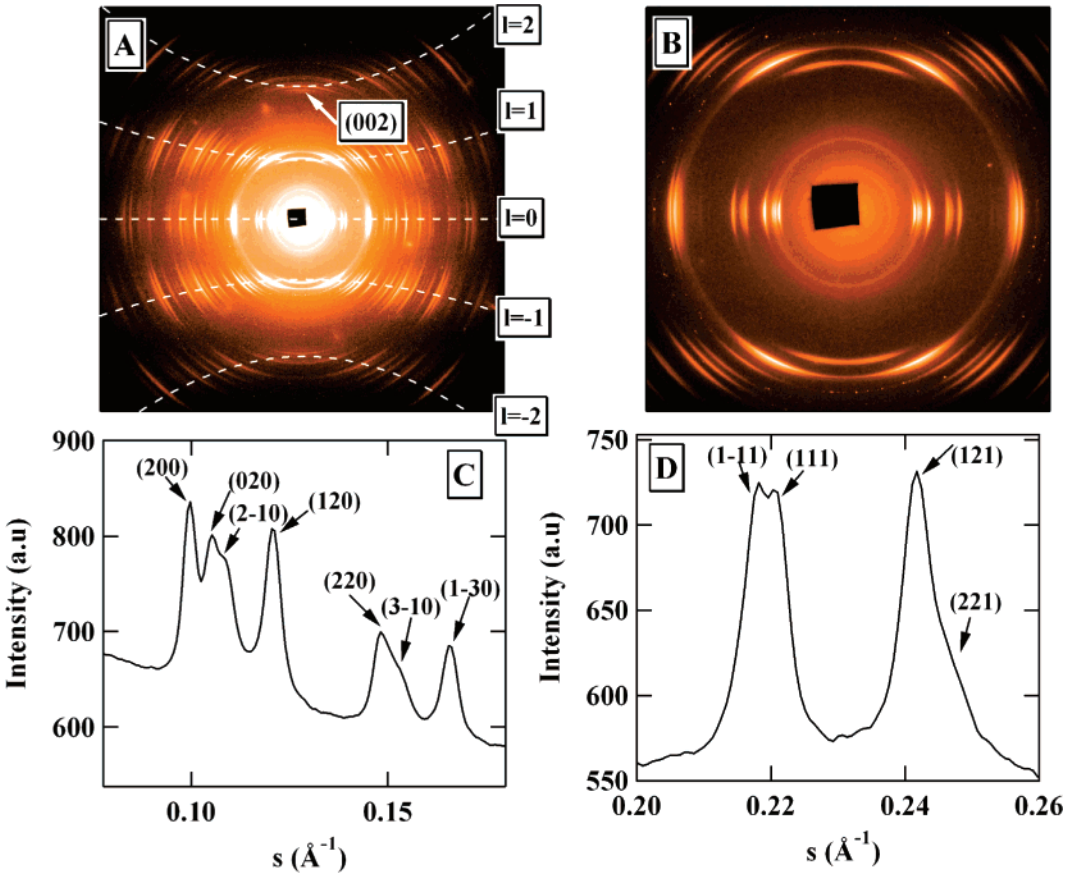

Figure 5. (A) X-ray fiber diffraction data of the β polymorph of PDPS recorded at −80 °C. The layer lines are indicated by dotted lines. (B) Zoom of the same pattern in the low angle range. (C) Equatorial intensities of the pattern in part A. (D) Intensities of the pattern in part A along the first layer line ($l = 1$).

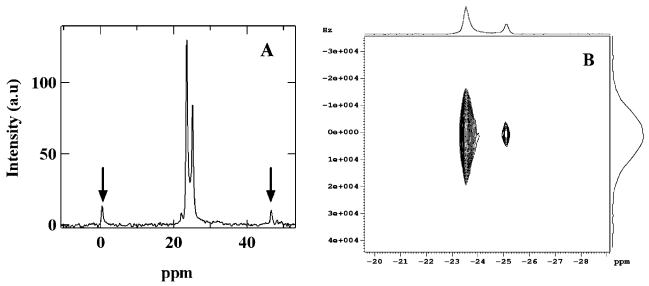

Figure 6. (A) ^{29}Si DD-MAS spectrum. (B) ^{1}H/^{29}Si 2D WISE NMR spectrum measured at ambient temperature.

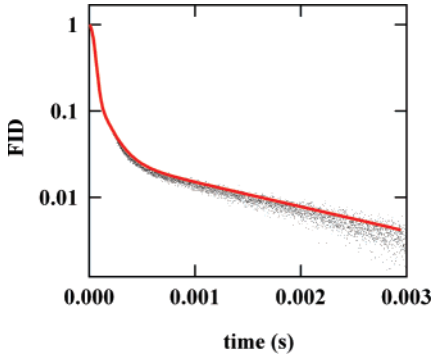

Figure 7. ^{1}H FID spectrum measured at ambient temperature and the corresponding fit with eq 2 in red.

to a phase with a mobility that is sufficiently high to average the dipolar interactions, while the second would correspond to a less mobile phase where the dipolar interaction between the silicon atoms and the protons is not averaged. To distinguish between these alternative interpretations ^{1}H/^{29}Si CP-WISE spectra were measured (Figure 6B). This technique adds to the ^{29}Si DD-MAS spectra information concerning the molecular dynamics of the system. It can be seen that the resonance at −23.52 ppm indeed corresponds to a less mobile part of the system and the one at −25.1 ppm to more mobile regions. All Si atoms in the sample thus appear to be in equivalent magnetic environments.

The FID spectrum is given in Figure 7. The curve exhibits three distinct regions revealing different mobilities and can be fitted with a sum of two exponential and one Gaussian functions according to

$$y = m_1 \exp(-m_2 t) + m_3 \exp(-m_4 t) + m_5 \exp(-(m_6 t)^2) \quad (3)$$

The m_2, m_4, and m_6 coefficients stand for the inverse of the characteristic decay times, while m_1, m_3, and m_5 give the relative weight of each of the functions. The values resulting from the fit are as follows: $m_1 = 2.5 \pm 1.0\%$, $m_3 = 20.5 \pm 1.0\%$, and $m_5 = 77.0 \pm 1.0\%$. The characteristic times are 1.53 ms, 124 μs, and 60 μs for the inverse of m_2, m_4, and m_6 coefficients, respectively. The last relaxation is much larger in the frequency domain and can be assigned to the crystalline regions. The crystallinity can then be estimated to be approximately 77%.

III.4. AFM Measurements. The semicrystalline morphology of PDPS films was studied on samples oriented by rubbing. To explore the influence of orientation of polymer chains prior to crystallization, the sample was rubbed either above or below the isotropization temperature followed by slow cooling to ambient temperature. During subsequent heating, temperature-resolved AFM was performed to follow the changes in the surface morphology upon the α-Col$_h$ transition.

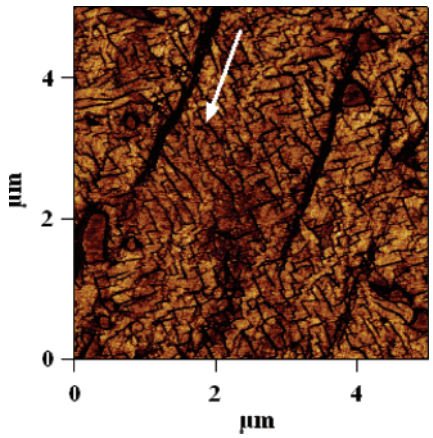

Figure 8. Room-temperature tapping mode AFM phase image (5 × 5 μm^2) of a PDPS sample prepared by rubbing. The rubbing was performed in the mesophase at 110 °C, i.e., far from the isotropization point, and was followed by quenching to ambient temperature.

III.4.1. Morphology of Thin Shear-Oriented Layers in the Crystalline and Mesomorphic State. Figure 8 shows the semicrystalline morphology, at ambient temperature, resulting from shearing of mesomorphic layers at 110 °C, i.e., well below the clearing point. The sample was annealed for 3 min after the shearing and cooled to room temperature at 10 °C·min^{-1}. The shearing produces gross features in the phase and height images in the form of dark stripes parallel to the shearing direction. The surface is almost entirely covered with crystalline domains in which numerous oriented lamellar blocks with distinct edges can be distinguished. These are oriented more or less perpendicularly to the rubbing direction, which is indicated by the arrow (Figure 8). This morphology looks similar to the "parquet"-like appearance of alkane layers in which the crystals are built up of fully extended chains.[30] Estimated from the images, the PDPS crystal thickness e is on the order of 100−150 nm, which indicates that the chains are in the nearly fully extended conformation (cf. Table 1).

Rubbing at 230 °C, i.e., well above the isotropization temperature, results in the droplet-like morphology shown in Figure 9. This morphology is believed to result from a competition of structure formation and dewetting. The observed droplet size distribution is rather broad, with the largest drops having diameters around 1.5 μm. At ambient temperature many drops reveal the internal structure with characteristic lamella-like stripes. The presence of these structures could indicate that the drops are partly mesomorphic (Figure 9C), which indicates

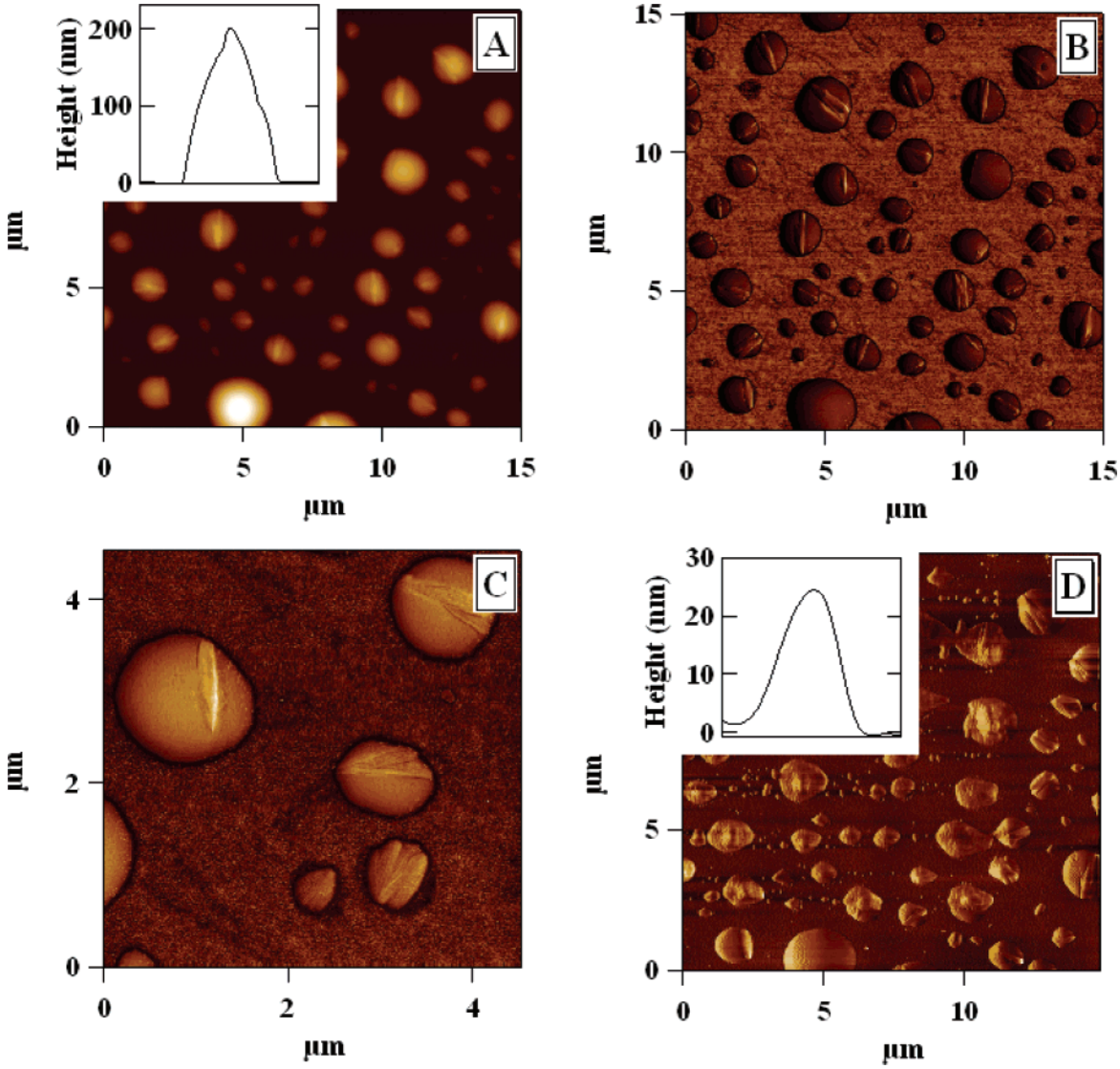

Figure 9. (**A**−**D**) AFM height and phase images of a thin PDPS layer, which was rubbed in the molten state at 230 °C) and cooled to room temperature: (A−C) light tapping; (D) hard tapping. Images A and D were recorded on the same region at ambient temperature; the image in part C is a zoom of part A. The insets in parts A and D show the height of the droplets.

a difference in phase behavior between the confined and the bulk polymer. It is well documented that typical bulk quenched PDPS samples are crystalline at ambient temperature due to rather high rates of mesophase formation and mesophase crystallization.[1] The appearance and stability of the partly mesomorphic or amorphous PDPS droplets drastically depends on the interaction force between the tip and the sample: in light tapping (small force) no visible deformation occurs (see Figure 9A−C), while in the hard tapping regime (Figure 9D) two important changes are observed. First, due to disintegration of the initial droplets, a large number of small droplets aligned in the scanning direction appear near the initial ones. Second, the topographical profile of the drops reversibly changes from about 200 (inset in Figure 9A) to approximately 20 nm (inset in Figure 9D) when the tapping regime is changed from light to hard. This deformability of the drops unequivocally demonstrates that they are not crystalline but mesomorphic at ambient temperature.

III.4.2. Morphological Changes Resulting from Reversible Crystal-Mesophase Transition. The change in sample morphology at the α-Col$_h$ transition was studied on a sample, which was initially prepared by rubbing in the mesophase at 110 °C followed by cooling to ambient temperature at a rate of 1.0 °C·min^{-1}. The resulting sample morphology at ambient temperature is shown in Figure 10A. On heating the crystalline blocks gradually disappear and, after complete melting, they transform in the typical mesomorphic lamellae. Figure 10B shows large lamellar bundles oriented nearly perpendicularly to the rubbing direction. On cooling the crystallization starts spontaneously. Thus, during isothermal scanning of the surface at 40 °C, the mesomorphic lamellae are rapidly covered by crystalline blocks. Crystallization of the undercooled mesomorphic PDPS can be also initiated by changing the tip−surface interaction force to switch from light to a hard tapping. In Figure 10C the lower part of the image is filled with crystalline blocks formed upon imaging in hard tapping at 40 °C. During the next scan the whole image becomes covered with crystals, with the morphology being practically identical to the initial one (Figure 10A). Very similar crystalllization behavior is observed during nonisothermal crystallization when the crystallization temperature is continuously decreased. The final semicrystalline morphologies of isothermally and nonisothermally crystallized mesomorphic PDPS are similar.

The morphology of the low molecular mass PDPS (sample II) was studied only in the crystalline state because of its much less pronounced mesomorphic behavior. Prior to observation, the sample was melted at about 100 °C and crystallized by cooling at approximately 45 °C. AFM height images (Figure 11) show a sample morphology consisting of stacks of lamellae with uneven edges, which are oriented at variable angles with respect to the surface. Estimates of the crystal thickness range from 15 and 25 nm, which is typical for a semicrystalline polymer.

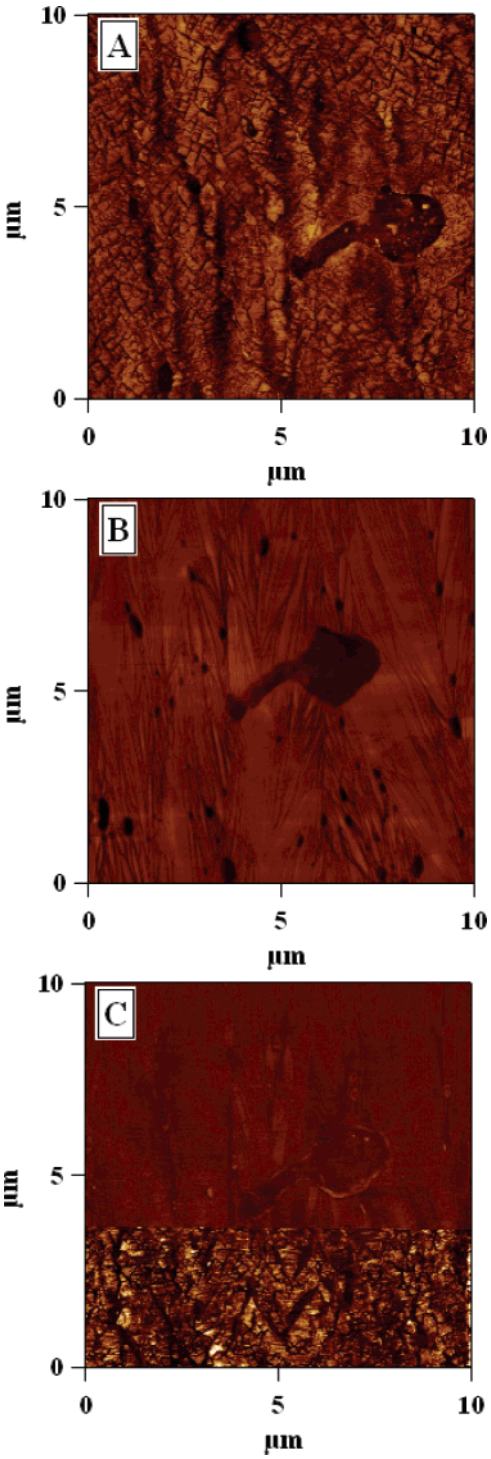

Figure 10. 10 × 10 μm^2 AFM phase images of the bulk PDPS sample recorded at different temperatures. (A) PDPS sample prepared by rubbing in the mesophase at 110 °C and slowly (1.0 °C·min^{-1}) cooled to room temperature. (B) Same region as in part A imaged at 81 °C (mesomorphic state). (C) Same region as in part A at 40 °C (crystallization of the mesophase).

IV. Discussion

IV.1. Structure of the α Crystal. The construction of the PDPS lattice was started from the chain backbone. The conformation of the backbone has to be close to the planar cis−trans, as evidenced by the *c* parameter (5.00 Å). This assumption is reinforced by the fact that for the β_2 polymorph of PDES, a similar value of the chain repeat was found (5.02 Å).[30] Generally, a trans zigzag conformation cannot be realized in linear siloxanes due to a significant difference between the valency angles of the O−Si−O and Si−O−Si bonds.[31] The cis−trans conformation of the main chains is also supported by the NMR results that are indicating that the environment for all Si atoms is equivalent. A similar conclusion was drawn in previous studies of PDMS.[32] These authors showed that the 2-fold helical conformation proposed by Damaschun[33] was incorrect based on the inconsistency of the expected conformational heterogeneity of the environment of Si atoms and the observation of a single resonant peak in ^{29}Si NMR spectra.

The symmetry group of the α lattice was deduced based on the selection rules for the observed reflections. The intensities

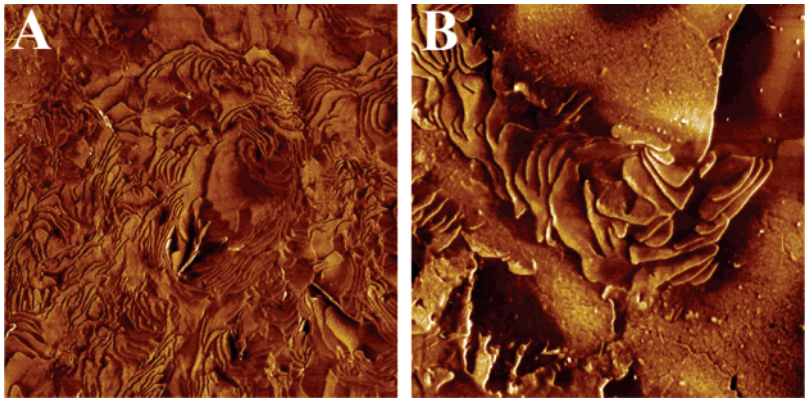

Figure 11. 20 × 20 (A) and 5 × 5 μm^2 (B) AFM phase images of the low molecular mass PDPS fraction, respectively. The sample was crystallized from the mesomorphic state at about 45 °C and slowly cooled to room temperature after crystallization.

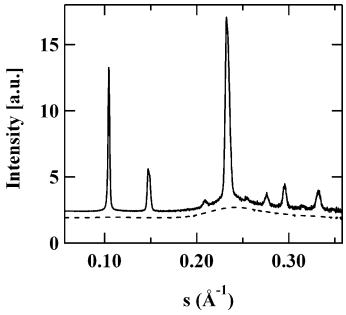

Figure 12. Experimental X-ray diffraction curve measured at room temperature (solid line) together with the amorphous halo (dashed line). The curves are vertically offset for clarity.

of the reflections together with sets of possible *hkl* indices corresponding to *d* spacings close to the experimental ones are given in Table 2. On the equator only *hk*0 reflections with $h,k = 2n$, *h*00 with $h = 2n$ and 0*k*0 with $k = 2n$ are present (Figure 4C). The meridional peaks 00*l* obey the extinction condition $l = 2n$. The indices of the first layer line peaks allowed to suggest that for all *hkl* reflections $h + k + l$ is even. The systematic absences imply the presence of a 2-fold screw axis along *c* and two glide planes perpendicular to *c* and parallel to *a* and *b*, respectively. The glides provide the required zonal reflection conditions for the equator. Altogether the observed extinction conditions cannot be satisfied by any of the tetragonal symmetry groups. Therefore, we suggest that the symmetry group is lower than tetragonal. An additional argument providing support to this hypothesis is that PDPS single crystals obtained from dilute solutions do not have the square habit,[11] typical of tetragonal lattices. Among the orthorhombic and monoclinic lattices the monoclinic space group *C*2/*c* (No. 15)[34] with *c*-unique satisfies all the above-mentioned selection rules. The extinction condition $h + k + l = 2n$ is met by cell choice three, as it has the appropriate lattice vector.

The refinement of the unit cell was performed by fitting the simulated diffraction intensity to the experimental amorphous background corrected powder diffraction curve (Figure 12). The initial setting angle of the backbone was determined by comparing the experimental and calculated structure factors for several intense equatorial peaks and was found to be close to either 0 or 90°. The molecular model was refined in three steps. First, the manually built structure was minimized using the *Smart Minimizer* algorithm while fixing the lattice parameters. Subsequently, the lateral chains conformation was refined by fitting the simulated diffractogram to the experimental curve by iteratively employing the Rietveld Refinement and Solve modules of the "Materials Studio" program. In the last step,

Table 4. Fractional Atomic Coordinates of the α Polymorph of PDPS at Room Temperature

atom	*x*	*y*	*z*
O	0.250	0.025	−0.145
Si	0.250	−0.046	0.038
C1	0.333	−0.094	−0.043
C2	0.393	−0.066	0.130
C3	0.463	−0.089	0.008
C4	0.173	−0.101	−0.047
C5	0.189	−0.178	0.025
C6	0.120	−0.220	0.029

Table 5. Geometrical Parameters of the Chain Conformation in the α Polymorph of PDPS

Bond Lengths, Å			
Si−O	1.631	C−C	1.540
Si−C	1.867		
Bond Angles, deg			
Si−O−Si	138.7	O−Si−C	109.5
O−Si−O	109.7	Si−C−C	109.5
C−Si−C	109.5	C−C−C	109.5
Torsion Angles, deg			
O−Si−C1−C2	−85.5	O−Si−C4−C5	−155.5
Si−C1−C2−C3	163.0	Si−C4−C5−C6	−164.5

the fractional atomic coordinates were fixed while the lattice parameters, the crystal size and the overall isotropic temperature factor were minimized using the Rietveld method. The final parameters of the lattice are $a = b = 19.125$ Å and $c = 4.994$ Å. These values are in good agreement with the ones obtained from the analysis of the fiber diffraction pattern. The values of the crystal size along *a* and *b* were kept equal because the resolution of the experimental data did not suffice to distinguish between them. The final geometrical parameters of the structure and the fractional atomic coordinates are given in Tables 4 and 5, respectively. The experimental and simulated X-ray diffraction intensities are compared in Figure 13. There is a good correspondence both for peak positions and intensities of the six strongest diffraction peaks. The agreement between the model and experiment is confirmed by a reasonable R_{wp} value of 0.127. The final crystalline structure, shown in Figure 14, contains the siloxane chains having all the same orientation with their planes parallel to the *b* direction, i.e., a setting angle of 90°. The lateral alkyl chains lie in the planes perpendicular to the chain axis, as can be seen on the *bc* projection of the unit cell (Figure 14B). The best agreement with the experimental diffraction pattern was achieved using the overall isotropic temperature factor *B* of 15.9 Å^2. This rather high value is explained by backbone mobility, which is due to the labile Si−O−Si bond angle.[32] The *B* value is however somewhat lower than the one previously reported for the case of PDES (28 Å^2),[30]

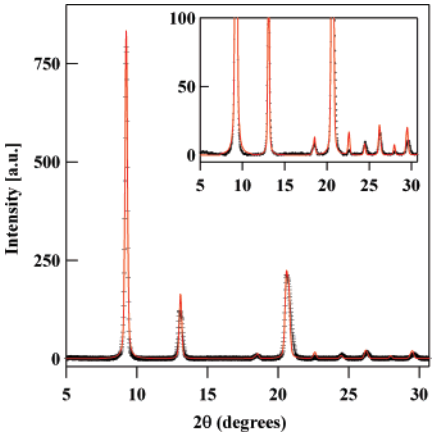

Figure 13. X-ray diffraction intensity of the α polymorph of PDPS corrected for the amorphous background (black line) and simulated diffraction intensity (red line). The inset gives a magnified view of low intensity reflections.

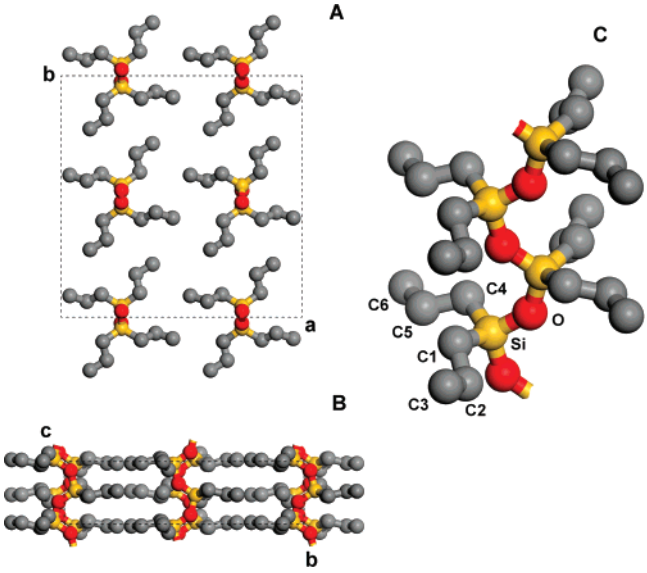

Figure 14. The α unit cell of PDPS viewed perpendicular to the *ab* plane (A) and perpendicular to the *ac* plane (B); the hydrogen atoms are removed for clarity. A fragment of the PDPS chain in cis-trans conformation (C).

which could reflect the reduced mobility of the backbone due to the steric effects caused by the longer side chains.[4]

It is instructive to calculate the diffracted intensity due to the electron-rich backbone and lighter side chains separately (Figure 15). It can be seen for example that the backbone provides dominant contributions to the (200)/(020) and (220) peaks, whereas the intensities of the (400)/(040)/(101)/(011) peaks located at about 18.5° in 2θ are comparable. Therefore, the weak intensity of this peak in the global structure is due to the opposite phases of the diffracted waves generated by the backbone and lateral chains.

IV.2. Semicrystalline Morphology and Chain Conformation in the Crystalline and Mesomorphic State. As pointed out in section III.2.2.2, the X-ray diffraction patterns corresponding to the crystalline phase of PDPS are atypical for polymers. They are characterized by sharp reflections and a weak amorphous halo, which suggests large crystal dimensions and high crystallinity of the sample. The calculation of crystallinity from the fit to the powder X-ray diffraction data after setting the disorder parameters to zero gives a crystallinity degree of 91%, which is unusually high for a semicrystalline

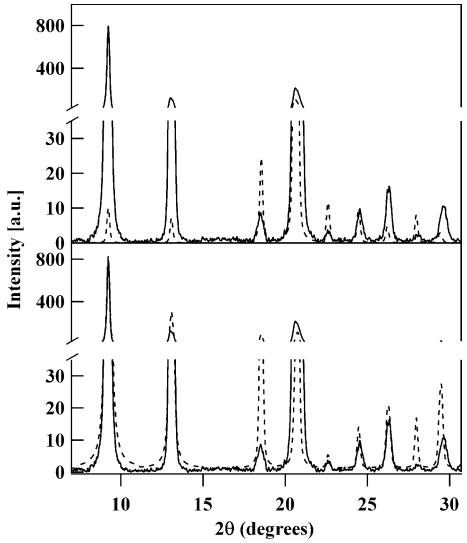

Figure 15. Calculated X-ray intensity (dashed lines) due to the main chain (bottom panel) and lateral alkyl chains (top panel) of the α unit cell of PDPS, respectively. The total simulated intensity (solid line) is given for comparison. The chain backbone mainly contributes to the strongest (200)/(020) and (220) equatorial peaks. The contributions of the backbone and lateral chains to the (400)/(040)/(101)/(011) reflections are comparable in amplitude and opposite in phase.

polymer in the bulk and even exceeds typical values for polymers crystallized from solution (e.g., single-crystal mats).[35] This high crystallinity is in qualitative accord with the densitometric data and is somewhat higher than the value found by solid-state NMR (77%). The discrepancy between the NMR and X-ray crystallinity values can be accounted for by uncertainty in assigning the fraction with intermediate mobility to the amorphous part of the sample alone.

Although the X-ray data do not allow the accurate determination of the crystal size by using the Scherrer broadening formula, it is possible to determine that the lower size limit is approximately 31 nm. AFM data show that the crystal thickness ranges from 100 to 150 nm and thus by far exceeds typical values for semicrystalline polymers. On the basis of this unusual thickness of the PDPS crystals in the bulk we can conclude that the polymer chains have an extended or nearly-extended chain conformation (cf. Table 1). Formation of extended chain polymer crystals is rare but was described for HDPE, crystallized from an hexagonal columnar mesophase under certain conditions.[36,37] In the case of HDPE, the individual polymer chains form cylindrical columns arranged on a hexagonal two-dimensional lattice. Similar to HDPE, the columnar mesophase of PDPS does not exhibit any long-range order along the column direction but only a lateral order of the chain axes.

Apart from HDPE, hexagonal columnar phases have been reported also for several other polymers such as 1,4-*trans*-polybutadiene (PBD),[38] polysilanes,[39−43] polysilylenemethylenes,[44] polyamides,[45] poly(dialkoxy phosphazenes),[46] rigid-rod polyesters,[47] and semifluorinated alkanes.[48] However, the semicrystalline morphology of these polymers, crystallized from hexagonal columnar phase, has not been studied in detail so far. Historically, PDES[49] and PBD[39] were probably the first polymers to display the hexagonal columnar mesophase at ambient pressure and in a relatively broad temperature range. Similarly to PDPS, PDES and PBD form very thick lamellae of about 150−300 nm, typical of extended chain crystals, when crystallized from the mesophase. It is evident that the mesomorphic pre-ordering of the chains enhances the crystallite thickness and that thermodynamically more stable crystals are

being formed. The efficiency of the mesophase-assisted crystallization for PDPS can be understood if one recalls that the chain diameters in the mesophase and in the crystal are very close and the orientation of the chains in the mesophase is not modified upon crystallization (cf. Figures 3 and 4). Therefore, crystal growth is expected to be templated by the structure formed by the mesomorphic columns.[15] Smaller values of lamellar thickness measured for the low molecular mass PDPS (sample II) could indicate that the crystallization is not mesophase-assisted but occurs according to the classical route, i.e., from a disordered state. This can be explained by the fact that the mesophase stability temperature window of the mesophase stability is much smaller (23 °C), compared to 135 °C for PDPS, and cooling of the sample from the melt, without annealing in the mesophase, could result in quenching of the amorphous state before the onset of crystallization.

V. Conclusions

The thermal behavior, crystalline structure, and semicrystalline morphology of poly(di-*n*-propyl siloxane), PDPS, were studied with X-ray powder and fiber diffraction, DSC, solid-state NMR and atomic force microscopy. It was found that PDPS, as a function of temperature, has two crystalline phases, α (−45.5 °C < T < 62 °C) and β (T < −45.5 °C), and a hexagonal columnar mesophase, which is stable in a broad temperature between ca. 62 and 197 °C. The low-temperature phase β is monoclinic with lattice parameters a = 20.60 Å, b = 19.22 Å, c = 4.95 Å, γ = 93.1°. The α crystalline modification has a pseudo-tetragonal unit cell with $a = b$ = 19.15 Å and c = 5.00 Å and is characterized by a monoclinic $C2/c$ (N° 15) space group. In the refined unit cell (R_{wp} = 0.127), found after crystallograpic refinement procedures have been applied, the PDPS chains adopt a planar cis−trans conformation with the plane of the chain parallel to the b axis and with the lateral chains lying in the planes perpendicular to the chain axis.

The results of X-ray and NMR studies indicate that PDPS crystallizes from the mesophase by forming a highly crystalline material with very thick (100−150 nm thick) crystalline lamellae corresponding to an extended or nearly-extended chain conformation. The semicrystalline morphology of the rubbed α crystal layers reveals a "parquet"-like appearance, similar to that found for alkane layers containing crystals with fully extended chains. This is a rare feature, which PDPS shares similar to materials such as HDPE crystallized at high pressures or 1,4-*trans*-poly(butadiene).

Acknowledgment. This work was financially supported by the Communauté Française de Belgique (ARC N 00/05-257), the RFBR (Grant 02-03-32199), INTAS (Grant 00-525), and the European Science Foundation (COST P12). The synchrotron radiation work was supported by the European Union through the HCMP Access to Large Installation Project, Contract HPRI-CT-1999-00017 to the EMBL-Hamburg. We are grateful to F. Meneau (BM26, ESRF) for the assistance in the X-ray measurements. We acknowledge Dr. M. Dupire and M. Debras (Atofina Research, Feluy, Belgium) for the help with the density measurements and F. Aussenac (Bruker Wissembourg, France) for the CP-WISE spectrum. Yu.K.G. is thankful to Digital Instruments/Veeco Metrology Group and the University of California at Santa Barbara (Prof. E. Kramer) for support of his research visit during which the AFM study was performed. The authors are grateful to Dr. B. Lotz for helpful discussions. B.G. is a postdoctoral fellow of the Fund for Scientific Research-Flanders (Belgium) (F.W.O.-Vlaanderen). The authors thank F.W.O.-Vlaanderen and Prof. H. Reynaers for their continuous support of the DUBBLE project.

References and Notes

(1) Godovsky, Yu. K.; Papkov, V. S. *Adv. Polym. Sci.* **1989**, *88*, 129.
(2) Molenberg, A.; Moeller, M.; Sautter, E. *Prog. Polym. Sci.* **1997**, *22*, 1133.
(3) Godovsky Yu. K.; Makarova, N. N.; Papkov, V. S.; Kuzmin, N. N. *Makromol. Chem. Rapid Comunn.* **1985**, *6*, 443.
(4) Godovsky Yu. K.; Mamaeva, I. V.; Makarova, N. N.; Papkov, V. S.; Kuzmin, N. N. *Makromol. Chem., Rapid Comunn.* **1985**, *6*, 797.
(5) Shulgin, A. I.; Godovsky, Yu. K. *Polym. Sci. USSR* **1987**, *29*, 2845.
(6) Godovsky, Yu. K.; Papkov, V. S. *Makromol. Chem., Macromol. Symp.* **1986**, *4*, 71.
(7) Shulgin, A. I.; Godovsky, Yu. K.; Makarova, N. N. *Thermochim. Acta* **1994**, *238*, 337.
(8) Out, G.; Turetskii, A.; Moeller, M. *Makromol. Chem., Rapid Commun.* **1995**, *16*, 107.
(9) Out, G.; Siffrin, S.; Frey, H.; Oelfin, D.; Koegler, G.; Moeller, M. *Polym. Adv. Technol.* **1994**, *5*, 796.
(10) Godovsky, Yu. K.; Papkov, V. S.; Magonov, S. N. *Macromolecules* **2001**, *34*, 976.
(11) Petersen, D. R.; Carter, D. R.; Lee, C. L. *J. Macromol. Sci. −Phys.* **1969**, *B3* (3), 519.
(12) Slottke, H. Die Konformation der mesophasenbildender Poly(di-*n*-alkylsiloxane), Ph.D. Thesis. University of Mainz, Germany, 1995.
(13) Molenberg, A.; Moeller, M. *Macromolecules* **1997**, *30*, 8332.
(14) Molenberg, A. Columnar morphologies of polysiloxanes and their block copolymers, Ph.D. Thesis. University of Ulm, Germany, 1997.
(15) Gearba, R. I.; Bondar, A.; Lehmann, M.; Goderis, B.; Bras, W.; Koch, M. H. J.; Ivanov, D. A. *Adv. Mater.* **2005**, *17*, 671.
(16) Magonov, S. N. Atomic Force Microscopy in Analysis of Polymers. In *Encyclopedia of Analytical Chemistry*; Meyers, R. A., Ed.; John Wiley & Sons Ltd.; Chichester, England, 2000; pp 7432−7491.
(17) Bras, W.; Dolbnya, I. P.; Detollenaere, D.; van Tol, R.; Malfois, M.; Greaves, G. N.; Ryan, A. J.; Heeley, E. *J. Appl. Crystallogr.* **2003**, *36*, 791.
(18) Bras, W.; Derbyshire, G. E.; Ryan, A. J.; Cooke, J.; Devine, A.; Komanschek, B. E.; Clark, S. M. *J. Appl. Crystallogr.* **1995**, *28*, 26.
(19) Blanton, T. N.; Barnes, C. L.; Lelental, M. *J. Appl. Crystallogr.* **2000**, *33*, 172.
(20) Klug, H. P.; Alexander, L. E. *X-ray Diffraction Procedures for Polycrystalline and Amorphous Materials*, 2nd ed.; John Wiley & Sons: New York, 1974.
(21) Magonov, S. N.; Godovsky, Yu. K. *Am. Lab.* **1999**, *31*, 52.
(22) Godovsky, Yu. K.; Magonov, S. N. *Langmuir* **2000**, *16*, 3459.
(23) Basire, C.; Ivanov, D. A. *Phys. Rev. Lett.* **2000**, *85*, 5587.
(24) Ivanov, D. A.; Amalou, Z.; Magonov, S. N. *Macromolecules* **2001**, *34*, 8944.
(25) Ivanov, D. A.; Magonov, S. Atomic Force Microscopy Studies of Semicrystalline Polymers at Variable Temperature. In *Polymer Crystallization: Observations, Concepts and Interpretations*; Sommer, J. U., Reiter, G., Eds.; Springer-Verlag: Berlin, 2003; pp 98−129.
(26) Magonov, S. N.; Godovsky, Yu. K. *Am. Lab.* **1998**, *30*, 15.
(27) Exploring the High-Temperature AFM and Its Use for Studies of Polymers. Ivanov, D. A.; Daniels, R.; Magonov, S. Application Note published by Digital Instruments/Veeco Metrology Group 2001; pp 1−12. Available on line at URL: http://di.com/APPNotes_PDFs/AN45%20HeatingStage.pdf.
(28) Tsvankin, D. Ya.; Papkov, V. S.; Zhukov, V. P.; Godovsky, Yu. K.; Svistunov, V. S.; Zhdanov, A. A. *J. Polym. Sci.: Polym. Chem. Ed.* **1985**, *23*, 1044.
(29) Inomata, K.; Yamamoto, K.; Nose, T. *Polym. J.* **2000**, *12*, 1044.
(30) Magonov, S. N.; Yerina, N. A.; Ungar, G.; Reneker, D. H.; Ivanov, D. A. *Macromolecules* **2003**, *36*, 5637.
(31) Flory, P. J. *Principles of Polymer Chemistry*; Cornell University Press: London, 1969.
(32) Schilling, F. C.; Gomez, M. A.; Tonelli, A. E. *Macromolecules* **1991**, *24*, 6552.
(33) Damaschun, V. G. *Kolloid-Z.* **1962**, *180*, 65.
(34) *International Tables for Crystallography*, 1st ed.; Kluwer Academic Publishers: Dordrecht, The Netherlands, 2002; Vol. A.
(35) Hocquet, S.; Dosière, M.; Thierry, A.; Lotz, B.; Dubreuil, N.; Koch, M. H. J.; Ivanov, D. A. *Macromolecules* **2003**, *36*, 8376.
(36) Bassett, D. C.; Khalifa, B. A.; Turner, B. *Nat. Phys. Sci.* **1972**, *239*, 106.
(37) Bassett, D. C.; Turner, B. *Nat. Phys. Sci.* **1972**, *240*, 146.
(38) Rastogi, S.; Ungar, G. *Macromolecules* **1992**, *25*, 1445.
(39) Lovinger, A. J.; Schilling, F. C.; Bovey, F. A. *Macromolecules* **1986**, *19*, 2660.
(40) Ungar, G.; Feijo, J. L.; Percec, V.; Yourd, R. *Macromolecules* **1991**, *24*, 953.

(41) Percec, V.; Zuber, M.; Ungar, G.; Alvarez-Castillo, A. *Macromolecules* **1992**, *25*, 1193.
(42) Klemann, B.; West, R.; Koutsky, J. *Macromolecules* **1993**, *26*, 1042.
(43) KariKari, E. K.; Greso, A. J.; Farmze, B. L.; Miller, R. D.; Rabolt, J. F. *Macromolecules* **1993**, *26*, 3937.
(44) Koopmann, F.; Frey, H. *Macromolecules* **1996**, *29*, 3701.
(45) Seitz, M.; Plesnivy, T.; Schimossek, K.; Edelmann, M.; Ringsdorf, H.; Fischer, H.; Uyama, H.; Kobayashi, S. *Macromolecules* **1996**, *29*, 6560.
(46) Papkov, V. S.; Il'ina, M. N.; Zhukov, V. P.; Tsvankin, D. Ja.; Tur, D. R. *Macromolecules* **1992**, *25*, 2033.
(47) Watanabe, J.; Sekine, N.; Nematsu, T.; Sone, M. *Macromolecules* **1996**, *29*, 4816.
(48) Percec, V.; Schlueter, D.; Ungar, G. *Macromolecules* **1997**, *30*, 645.
(49) Obolonkova, E. S.; Papkov, V. S. *Vysokomol. Soedin. (USSR)* **1990**, *31B*, 691.

MA0513315